Ginkgolide C alleviates atherosclerosis via activating Nrf2 to inhibit ROS-dependent NLRP3 inflammasome activation

RUI ZHANG

Department of Pharmacy, Shandong Provincial Hospital
Affiliated to Shandong First Medical University, Jinan, Shandong 250021, P.R. China

Received August 14, 2025; Accepted December 10, 2025

DOI: 10.3892/ijmm.2026.5746

Abstract. Atherosclerosis (AS), a chronic vascular pathology characterized by endothelial dysfunction, arises from the interplay of lipid dysregulation, oxidative stress, and inflammatory activation. Reactive oxygen species (ROS) overproduction triggers Nod-like receptor protein 3 (NLRP3) inflammasome signaling, exacerbating inflammatory cascades that drive plaque progression. The nuclear factor erythroid 2-related factor 2 (Nrf2)-mediated antioxidant pathway serves as a critical counterbalance to ROS/NLRP3 axis dysregulation, positioning pharmacological Nrf2 activation as a promising therapeutic strategy. The present study investigated the anti-atherosclerotic potential of ginkgolide C (GC), a terpene lactone from *Ginkgo biloba* with established anti-inflammatory and anti-ischemia/reperfusion injury properties, through coordinated modulation of redox-inflammatory pathways. Complementary *in vivo* (high-fat diet/vitamin D_3-treated $ApoE^{-/-}$ mice) and *in vitro* (oxidized-low density lipoprotein-stimulated aortic endothelial cells) models were established. Comprehensive analyses included histopathological characterization, lipid profiling, ultrastructural examination, redox-inflammatory biomarker quantification, and molecular pathway validation. GC significantly attenuated hyperlipidemia and plaque progression while preserving vascular ultrastructure. Mechanistically, GC enhanced endothelial survival through dual pathway modulation: i) Nrf2 nuclear translocation upregulated antioxidant enzymes [heme oxygenase-1/NAD(P)H quinone oxidoreductase 1/glutamate-cysteine ligase modifier subunit], restoring redox homeostasis; ii) NLRP3 inflammasome inhibition via Caspase-1 suppression mitigated inflammatory cytokine release. The present study demonstrated GC's dual-target therapeutic efficacy against AS through Nrf2-mediated oxidative stress resolution and NLRP3 inflammasome inactivation, offering new insights into phytochemical-based cardiovascular interventions.

Correspondence to: Professor Rui Zhang, Department of Pharmacy, Shandong Provincial Hospital Affiliated to Shandong First Medical University, 324 Jingwu Road, Huaiyin, Jinan, Shandong 250021, P.R. China
E-mail: 37725989@qq.com

Key words: ginkgolide C, atherosclerosis, nuclear factor erythroid 2-related factor 2, reactive oxygen species, Nod-like receptor protein 3

Introduction

Cardiovascular disease (CVD) persists as a foremost contributor to global morbidity and mortality, posing a pervasive disease burden that critically undermines population health metrics (1). Atherosclerosis (AS), serving as the pathological foundation and primary etiology of CVD, manifests as a chronic vascular disorder characterized by lipid-laden arterial wall deposition coupled with persistent oxidative stress and inflammatory responses (2,3). The pathogenesis of AS involves multiple processes: endothelial dysfunction, lipoprotein retention, macrophage activation, inflammatory cytokine release, oxidized low density lipoprotein (ox-LDL)-driven foam cell formation and vascular smooth muscle cell migration. Oxidative stress plays a central role by impairing endothelial function, promoting ox-LDL accumulation, and enhancing foam cell formation, collectively accelerating plaque development (4). These molecular interactions synergistically drive plaque instability through matrix metalloproteinase activation and fibrous cap attenuation. Preserving redox balance therefore represents a critical therapeutic strategy for decelerating atherogenesis and sustaining vascular homeostasis.

Under pathophysiological stress, the excessive production of reactive oxygen species (ROS) that surpasses the endogenous antioxidant capacity perturbs redox homeostasis, thereby inducing oxidative modifications to cellular nucleic acids, proteins, and lipids, which culminate in multi-level tissue damage (5). Substantial evidence identifies vascular endothelial dysfunction as the seminal event in atherosclerotic pathogenesis (6). Under physiological conditions, the vascular endothelium sustains homeostatic balance via orchestrated regulation of vasomotor tone, thrombotic homeostasis, and selective permeability. During atherosclerotic initiation, ROS-driven oxidative stress disrupts this equilibrium, manifesting as: i) Structural barrier compromise, ii) loss of thromboresistant capacity, and iii) transition to pro-inflammatory phenotype (7). This pathognomonic triad

perpetuates a vicious cycle of endothelial activation, subendothelial lipoprotein retention, and vascular remodeling that drives atherosclerotic plaque progression.

Nuclear factor erythroid 2-related factor 2 (Nrf2), the key transcriptional regulator of cellular redox balance, coordinates intrinsic antioxidant mechanisms to neutralize ROS-driven oxidative damage (8). Vascular endothelium employs tonic Nrf2 signaling to mediate oxidation-sensitive activation, orchestrating cytoprotective transcriptional programs through redox-responsive gene networks. Nrf2 deficiency dysregulates adaptive redox homeostasis, amplifying free radical flux and compromising reparative angiogenesis via blunted endothelial tip cell specification and dysfunctional angiocrine signaling (9). Under redox homeostasis, Keap1 orchestrates Nrf2 cytoplasmic retention by directing constitutive ubiquitination-proteasome turnover, thereby enforcing Nrf2 transcriptional dormancy. Electrophilic stress initiates redox-gated conformational switches within the Keap1-Nrf2 axis via cysteine sensor modification, uncoupling ubiquitin ligase activity while liberating Nrf2 for nuclear import. Nrf2 forms heterodimers with small Maf proteins in the nucleus, activating the expression of heme oxygenase-1 (HO-1), NAD(P)H quinone oxidoreductase 1 (NQO1) and glutamate-cysteine ligase modifier subunit (GCLM) through binding to antioxidant response elements (ARE) (10,11). This regulated genetic response orchestrates a reduction in ROS production, a bolstering of free radical scavenging capacity, and a stabilization of the intracellular redox state, thereby attenuating oxidative tissue damage.

The Nod-like receptor protein 3 (NLRP3) inflammasome serves as a molecular signaling nexus that integrates stress-activated pathways with inflammatory cascades, functionally linking canonical pyroptosis to atherosclerotic pathogenesis through regulated secretion of pro-inflammatory cytokines (12). Excessive ROS act as potent activators of the NLRP3 inflammasome, triggering its oligomerization through protein-protein interactions to form the NLRP3-ASC-pro-cysteinyl aspartate specific proteinase (Caspase-1) supramolecular complex (13). Activated Caspase-1 subsequently cleaves pro-Interleukin-1β (IL-1β) and pro-Interleukin-18 (IL-18) into their biologically active forms, driving the secretion of these inflammatory mediators while simultaneously inducing cellular osmotic imbalance through gasdermin-D-mediated membrane pore formation (14). This dual mechanism mediates the execution of distinctive pyroptotic events-cellular swelling, plasma membrane rupture, and release of cytoplasmic contents-the dissemination of which, as damage-associated molecular patterns, thereby potentiates inflammatory responses. The cyclical interplay between ROS overproduction, NLRP3 inflammasome activation, and persistent inflammation establishes a self-perpetuating vicious cycle that exacerbates vascular endothelial dysfunction and plaque instability in AS (15). Therapeutic strategies targeting ROS-dependent NLRP3 inflammasome activation demonstrate significant potential to disrupt this deleterious cycle, thereby attenuating inflammatory burden and ameliorating atherosclerotic progression.

Ginkgo biloba L. (Ginkgoaceae; MPNS-verified) a unique tree species native to China, is valued for its neuroprotective properties in addressing cardio-cerebrovascular diseases and neurological disorders (16). Contemporary pharmacological research has elucidated the multifaceted pharmacodynamics of foliar extracts, demonstrating their capacity to confer dose-dependent cardioprotection, modulate neurovascular homeostasis, and suppress neoplastic proliferation (17). Of particular scientific interest is ginkgolide C (GC) (Fig. 1), a unique terpenoid trilactone isolated from *Ginkgo biloba* leaves characterized by its distinctive pentacyclic structure. Previous studies have characterized GC as a pleiotropic therapeutic agent, demonstrating potent anti-inflammatory efficacy and the capacity to confer multi-organ protection in experimental models of cardiac and cerebral ischemia-reperfusion injury (18,19). Atherosclerotic progression is increasingly recognized as a critical pathogenic link between ischemic events and cerebral/cardiovascular comorbidities, driven by interconnected pathways of endothelial dysfunction and amplified oxidative stress (20). However, the potential of GC to mitigate atherosclerotic lesions through suppression of ROS-induced NLRP3 inflammasome activation and subsequent attenuation of inflammatory cascades remains experimentally unestablished.

The present study aimed to elucidate the anti-atherosclerotic mechanisms of GC through a combined experimental approach both *in vivo* and *in vitro*, focusing specifically on its dual-pathway regulatory activity. The experimental findings demonstrated that GC ameliorates atherosclerotic pathology through endothelial Nrf2 pathway activation, which coordinates upregulation of antioxidant defense proteins, suppression of ROS generation and sequential inhibition of NLRP3 inflammasome assembly, ultimately attenuating pro-inflammatory cytokine production and inflammatory cascade propagation.

Materials and methods

Materials and reagents. GC (PubChem CID: 161120) and Atorvastatin (AVT; PubChem CID: 60823) were commercially acquired from MilliporeSigma-Aldrich. Anti-NLRP3 (cat. no. 15101S) was obtained from Cell Signaling Technology, Inc. Anti-Nrf2 (cat. no. 16396-1-AP) was obtained from Proteintech Group, Inc. Anti-HO-1 (cat. no. PAA584Hu01), anti-NOQ1 (cat. no. PAL969Hu01), anti-GCLM (cat. no. PAB038Hu01), anti-Caspase-1 (cat. no. PAB592Hu01), anti-β-actin (cat. no. PAB340Mi01) and anti-histone (cat. no. PAS091Ge01) antibodies were obtained from Cloud-Clone Corp. The following analytical-grade materials were commercially sourced from Beyotime Institute of Biotechnology: BCA protein quantification kits (cat. no. P0010S), PVDF western blot membranes (cat. no. FFP28), SDS-PAGE electrophoresis systems (cat. no. PG012) and ECL Plus chemiluminescence substrates (cat. no. P0018M).

Randomization and blinding procedures. Randomization was applied to animal/cell grouping, and blinding was strictly maintained during data collection and analysis to minimize potential bias and ensure experimental objectivity.

Animal experiments. A total of 6 4-6-week-old male C57BL/6 mice weighing 14-16 g and 30 Apolipoprotein E-deficient ($ApoE^{-/-}$) male mice weighing 14-16 g were obtained from Huazhong Agricultural University and Guangdong Yaokang

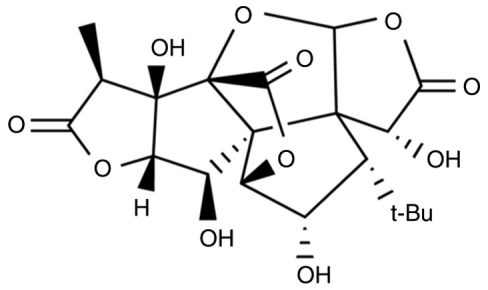

Figure 1. Chemical structure of ginkgolide C.

Biotechnology Co., Ltd., respectively. All animals were maintained under standardized laboratory conditions. Ambient temperature was regulated at 20-25˚C, relative humidity was stabilized at 40-60%, and a 12-h photocycle was enforced. A certified rodent diet and water were provided *ad libitum*. All experimental procedures strictly adhered to the Ethics Committee of the Shandong Provincial Hospital Affiliated to Shandong First Medical University (approval no. 2022-661; Jinan, China).

Mice were randomized into 6 groups (n=6/group): control group, AS model group, 2.5 mg/kg AVT group, and 12, 24, 48 mg/kg GC groups. ApoE$^{-/-}$ mice used for AS modeling, AVT and GC treatment underwent disease induction through three sequential interventions: Initial preconditioning via a single cholecalciferol injection (300,000 IU/kg in 0.2 ml saline), followed by 16 weeks of high-fat/high-cholesterol diet (40% of calories from fat), and culminating in a final intraperitoneal administration of vitamin D_3 (100,000 IU/kg). Control mice were maintained on standard chow and purified water under controlled environmental conditions (22±1˚C, 55±5% humidity, 12-h light cycle) throughout the study. After confirming successful AS development, daily tail vein injections of AVT or GC were administered continuously for 7 days to the AVT or GC groups. At the end of the experiment, euthanasia was performed by an intraperitoneal injection of an overdose of sodium pentobarbital (150 mg/kg). Death was confirmed by the cessation of heartbeat and respiration, assessed by visual inspection and palpation.

Plaque assessment. After 24-h fixation in 4% paraformaldehyde at 4˚C, aortic root specimens were dehydrated in 30% sucrose and embedded in OCT compound in the coronal orientation. Serial 10-μm-thick sections were obtained along the aortic valve axis using a cryostat. For analysis, 10 representative sections were stained with Oil Red O (Sigma-Aldrich) for lipid visualization or with hematoxylin and eosin (H&E) for structural assessment. Plaque areas were quantified in ImageJ software (version 1.8.0; National Institutes of Health) applying standardized threshold parameters.

Transmission electron microscope (TEM) observation. Aortic root specimens were primarily fixed with 3% glutaraldehyde in phosphate buffer (Ph 7.2) for 48-72 h, followed by thorough PBS rinsing and subsequent graded ethanol dehydration. Following embedding and polymerization in Epon 812 resin, tissue blocks were subjected to ultrathin sectioning. Sections of 90 nm thickness, prepared with an ultramicrotome equipped with a diamond knife, were imaged using a Hitachi H-800 TEM at an acceleration voltage of 80 kV to assess ultrastructural details.

Immunofluorescence (IF) staining. IF analysis cellular localization of Nrf2 and NLRP3 was assessed through IF. Fixed cells (pre-cooled methanol, -20˚C, 10 min) underwent triple PBS washing (5 min each, pH 7.4) followed by non-specific binding blockade with 3% BSA (MilliporeSigma)/0.1% Tween-20 (1 h, RT). Primary antibodies included anti-Nrf2 (1:200; cat. no. ab62352; Abcam) and anti-NLRP3 (1:500; cat. no. ab263899; Abcam). Corresponding Secondary antibodies (1:500; cat. nos. ab205718 and ab97051 Abcam) were purchased from Abcam. Nuclear visualization employed DAPI staining (0.1 μg/ml PBS; 5 min; cat. no. ab285390; Abcam). Confocal microscopy (Leica TCS SP8, 40x oil lens, NA 1.30) captured images using LAS X 3.7.4 with standardized 358/461 nm excitation/emission and z-axis imaging (1-μm intervals).

Serum lipid quantification. Blood samples were centrifuged at 2,000 x g for 20 min at 4˚C, followed by a 1:1 dilution of the resulting supernatant with phosphate-buffered saline (PBS). Total cholesterol (TC), triglycerides (TG), low-density lipoprotein cholesterol (LDL-C) and high-density lipoprotein cholesterol (HDL-C) were tested using a Beckman DXC700au system (NIST SRM 1951c-calibrated) with endpoint analysis at 500 nm under standardized conditions (37±0.2˚C, <3% intra-assay CV).

Cell experiments. Primary mouse aortic endothelial cells (MAECs) were obtained through enzymatic digestion of thoracic aortas isolated aseptically from 8-12-week-old mice. Following the removal of adventitial tissue and longitudinal incision, vessels were enzymatically digested with collagenase I (1 mg/ml) at 37˚C for 15-20 min. Digested cells were filtered through 40-μm strainers and plated onto gelatin-coated dishes in endothelial-specific medium (10% FBS; 30 μg/ml ECGS; 100 μg/ml heparin; all from Gibco; Thermo Fisher Scientific, Inc.). Cellular purity was enhanced through differential adhesion (three sequential 30-min platings at 37˚C, 5% CO_2). Cells were maintained in DMEM (Gibco; Thermo Fisher Scientific, Inc.) supplemented with 10% heat-inactivated fetal bovine serum and 1% penicillin/streptomycin (Gibco; Thermo Fisher Scientific, Inc.). Cultures were kept at 37˚C under a 5% CO_2 atmosphere with 95% humidity in a tri-gas incubator (Thermo Fisher Scientific, Inc.). To simulate atherosclerotic inflammatory responses, confluent monolayers were sequentially challenged with ox-LDL (100 μg/ml, 12 h).

The cells were randomized into 5 groups (n=3/group): control group, cells in DMEM without ox-LDL stimulation; Model group, cells treated with ox-LDL stimulation; GC group, cells pretreated with GC (1, 10, 100 μM) for 24 h prior to ox-LDL co-stimulation.

Cell viability. The assessment of cell viability was performed using the MTT reduction method. Interventions were performed upon the cells reaching a density of 5,000 cells per well. Following experimental interventions, the culture medium was replaced with 5 mg/ml MTT solution and

incubated at 37˚C for 4 h. Subsequently, the supernatant was carefully removed, and the formazan crystals were solubilized in DMSO under 300 rpm orbital agitation for 15 min. The optical density at 490 nm was recorded with a microplate reader and normalized relative to the control group.

ROS assay. ROS levels were measured via 2',7'-dichlorofluorescein diacetate (DCFDA; Abcam). Cells ($1x10^5$ cells/well) in 6-well plates were incubated with 10 μM DCFDA at 37˚C for 20 min. Fluorescence images were captured with a fluorescence microscope (BD Biosciences), and ROS fluorescence intensity was analyzed using Image-Pro Plus software (version 6.0; Media Cybernetics Inc.).

Detections of inflammatory factors and oxidative stress factors. IL-1β, IL-18 and tumor necrosis factor (TNF)-α concentrations in serum and cell culture supernatants were determined by ELISA kits (IL-1β, cat. no. 88-7013A-88; IL-18, cat. no. KMC0181; TNF-α, cat. no. BMS607-3; Thermo Fisher Scientific, Inc.) following the manufacturer's instructions. The levels of superoxide dismutase (SOD; cat. no. A001-3), malondialdehyde (MDA; cat. no. A003-1), lactate dehydrogenase (LDH; cat. no. A020-2), creatine kinase (CK; cat. no. A032-1-1), catalase (CAT; cat. no. A007-1-1), glutathione (GSH; cat. no. A006-2-1) and NADPH (cat. no. A115-1-1) in serum and cell culture supernatants were detected by chemical kits of Nanjing Jiancheng Engineering Institute.

TUNEL staining. DNA fragmentation in individual cells was detected by TUNEL staining with a fluorescence kit (Roche Diagnostics). Following fixation with 4% paraformaldehyde (20 min) and permeabilization with 0.1% Triton X-100 (10 min) at room temperature, MAECs on coverslips were subjected to TUNEL assay by incubation with the reagent at 37˚C for 60 min. Fluorescent signals were visualized and recorded with an Olympus FV3000 confocal microscopy system.

Western blot analysis for Nrf2, NLRP3, HO-1, NQO1, GCLM and Caspase-1 expression levels in MAECs. Total protein quantification was performed using BCA assay. Subcellular fractionation was conducted with a Nuclear-Cytoplasmic Protein Isolation Kit (cat. no. P1250; Applygen Technologies, Inc.) following established protocols. Protein samples (50 μg) underwent SDS-PAGE (10% gel) electrophoresis and subsequent PVDF membrane transfer. Membranes were blocked with 5% non-fat milk at room temperature for 1 h, then incubation with primary antibodies (1:800 dilution) targeting Nrf2, NLRP3, HO-1, NQO1, GCLM and total Caspase-1 at 37˚C for 4 h. Membranes were subsequently probed with HRP-conjugated secondary antibodies diluted at 1:1,000. Specific signals were visualized with ECL Plus reagent and quantified via densitometry using a Bio-Rad Gel Imaging System and Quantity One software (version 5.0; Bio-Rad Laboratories, Inc.).

Total protein quantification was determined via BCA assay. Nuclear-cytoplasmic fractionation employed the nuclear-cytoplasmic protein isolation kit (cat. no. P1250; Applygen Technologies, Inc.) according to the manufacturer's instructions. A total of 50 μg protein samples were separated through SDS-PAGE and electrotransferred onto PVDF membranes. After 5% skim milk blocking, membranes were probed with primary antibodies (Nrf2/NLRP3/HO-1/NQO1/GCLM/Caspase-1; 1:800) at 37˚C (4 h), followed by HRP-secondary antibodies (1:1,000). Chemiluminescent detection was performed with ECL Plus reagent, followed by densitometric analysis of the bands using the Quantity One software (version 5.0; Bio-Rad Laboratories, Inc.) imaging system.

Statistical analysis. Triplicate experimental data are expressed as the mean ± SD. Intergroup comparisons were assessed through one-way ANOVA with Bonferroni post hoc adjustment (GraphPad Prism version 5.0; Dotmatics). $P<0.05$ was considered to indicate a statistically significant significance.

Results

GC alleviates atherosclerotic pathological damage in AS model mice. To observe the histopathological changes in the aortic root following atherosclerotic injury, H&E staining was performed. As depicted in Fig. 2A, aortic sections from the control group demonstrated a well-defined trilaminar architecture: The tunica intima was lined by a continuous endothelial monolayer; the tunica media showed regularly arranged, wavy elastic fibers interspersed with smooth muscle cells; and the tunica adventitia was composed of loose connective tissue. No pathological alterations such as lipid deposition, foam cell formation, inflammatory infiltration, luminal disruption, or vascular wall thickening were observed. In the model group (Fig. 2B), marked intimal thickening was observed, featuring foam cells (vacuolated cytoplasm), cholesterol clefts, inflammatory infiltration, and fibrous caps overlying lipid cores. The tunica media showed fragmented elastic fibers with reduced smooth muscle cells, while the adventitia presented neovascularization and chronic inflammation, accompanied by a narrowed and irregular lumen. In 2.5 mg/kg AVT group (Fig. 2C) and 12, 24, 48 mg/kg GC groups (Fig. 2D-F), the aortic intima displayed a significant decrease in pathological thickening with parallel reductions in atherosclerotic plaque deposition (Fig. 2G).

GC reduces atherosclerotic lipid deposition in AS model mice. To investigate the effect of GC on lipid deposition and examine its impact on plaque characteristics following atherosclerotic injury, Oil Red O staining was performed. As shown in Fig. 3A, the control group exhibited no Oil Red O-positive red signals in any aortic wall layers (intima, media, adventitia), with only physiological lipid staining observed in periadventitial adipose tissue. The luminal surface appeared smooth without lipid droplet adhesion, indicating no pathological lipid deposition. By contrast, the model group displayed bright red mass-like lipid deposits (plaque lipid cores) in the aortic sinus and subintimal regions, accompanied by diffuse punctate red infiltration (early lipid infiltration) at plaque margins. Strongly positive lipid halos surrounded cholesterol clefts in some areas, suggesting lipid metabolic disturbances and extensive foam cell aggregation (Fig. 3B). However, Oil Red O staining demonstrated a reduction in lipid core size, significant attenuation of red-positive deposition area, and faded lipid halos surrounding cholesterol clefts, indicative of ameliorated lipid

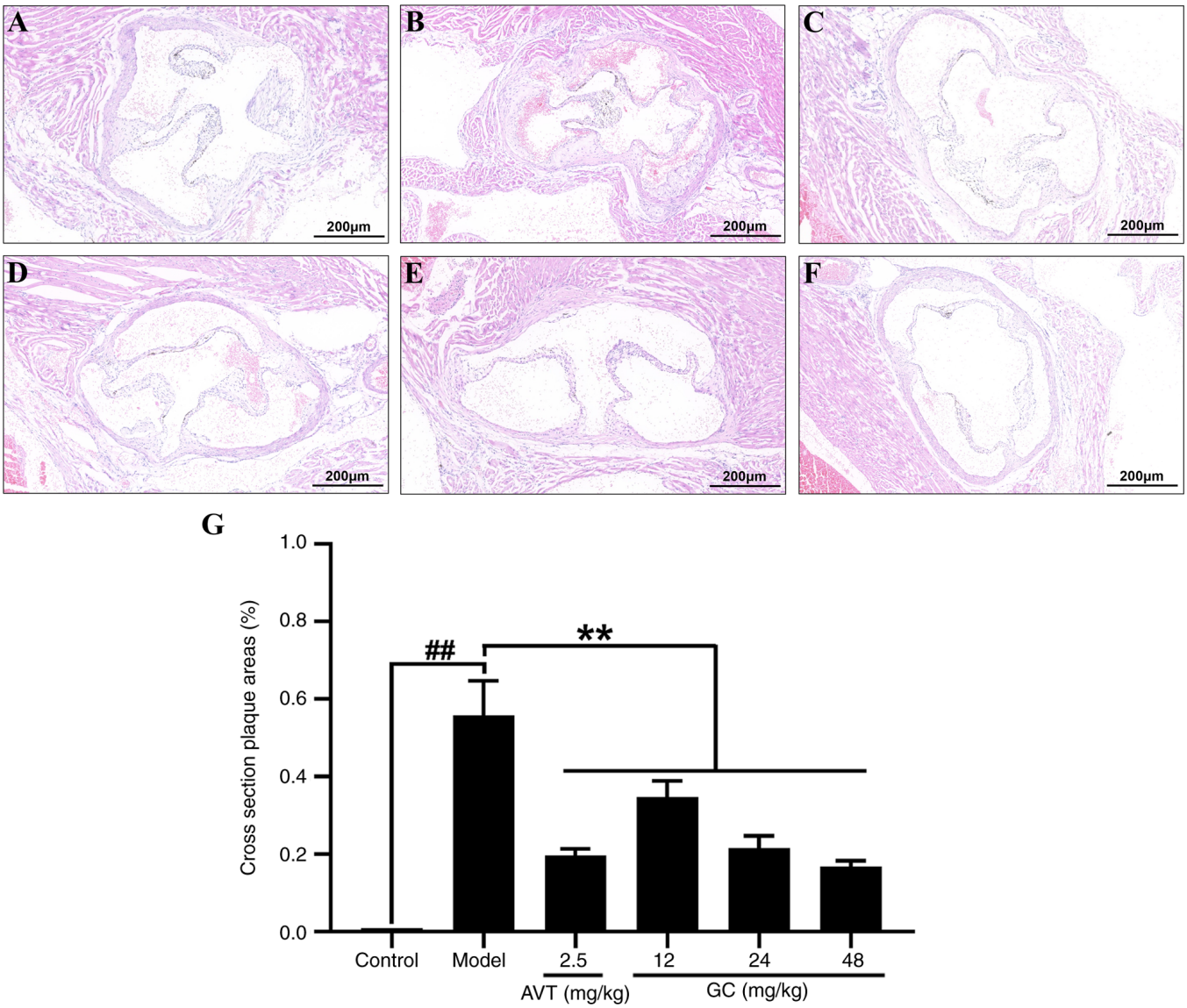

Figure 2. Effect of GC on histopathology of the aortic root via H&E staining in atherosclerosis model mice. Light microscopy images (magnification, x40) of aortic roots stained with H&E. (A) Control group, (B) model group, (C) 2.5 mg/kg AVT group, (D) 12 mg/kg GC group, (E) 24 mg/kg GC group and (F) 48 mg/kg GC group. (G) Quantitative analysis of atherosclerotic plaque area based on H&E staining. Data are expressed as the mean ± SD. $^{\#\#}$P<0.01 vs. control group; **P<0.01 vs. model group. GC, ginkgolide C; AVT, atorvastatin.

metabolic dysregulation and enhanced plaque stability after treatment of 2.5 mg/kg AVT (Fig. 3C) and 12, 24, 48 mg/kg GC (Fig. 3D-F). Quantitative analysis of atherosclerotic plaque area based on oil red O staining is demonstrated in Fig. 3G.

GC reduces blood lipid levels in AS model mice. The result in Table I showed that the blood lipid levels in model group were markedly changed (TG: 5.58±0.26 mM; TC: 41.59±5.49 mM; LDL-C: 16.14±2.41 mM and HDL-C: 1.46±0.24 mM, all P<0.01 vs. control group). 2.5 mg/kg AVT and 12, 24, 48 mg/kg GC significantly improved the blood lipid levels (all P<0.01 vs. model group). The findings revealed that GC exhibited hypolipidemic effects and attenuated atherosclerotic development.

GC improves atherosclerotic ultrastructural changes in AS model mice. Additionally, ultrastructural changes induced by GC were analyzed by TEM. In control group, the endothelial cells formed a continuous monolayer with intact tight junctions; the medial smooth muscle cells were densely packed with contractile myofilaments and surrounded by orderly arranged elastic fibers; the extracellular matrix showed no lipid droplet deposition, inflammatory infiltration, or structural disruption (Fig. 4A). However, in the model group, endothelial disruption with lipid deposition, smooth muscle foam cell transformation (marked by contractile myofilament loss and lipid droplet-induced organelle compression), and elastic fiber fragmentation were prominently observed. Concurrently, extracellular collagen disorganization and cholesterol crystal deposition synergistically drove plaque instability (Fig. 4B). The results in Fig. 4C-F revealed that 2.5 mg/kg AVT and 12, 24, 48 mg/kg GC significantly improved the endothelial continuity restoration, smooth muscle contractile phenotype reconstruction (marked by myofilament regeneration and lipid droplet clearance), and elastic-collagen reorganization in the

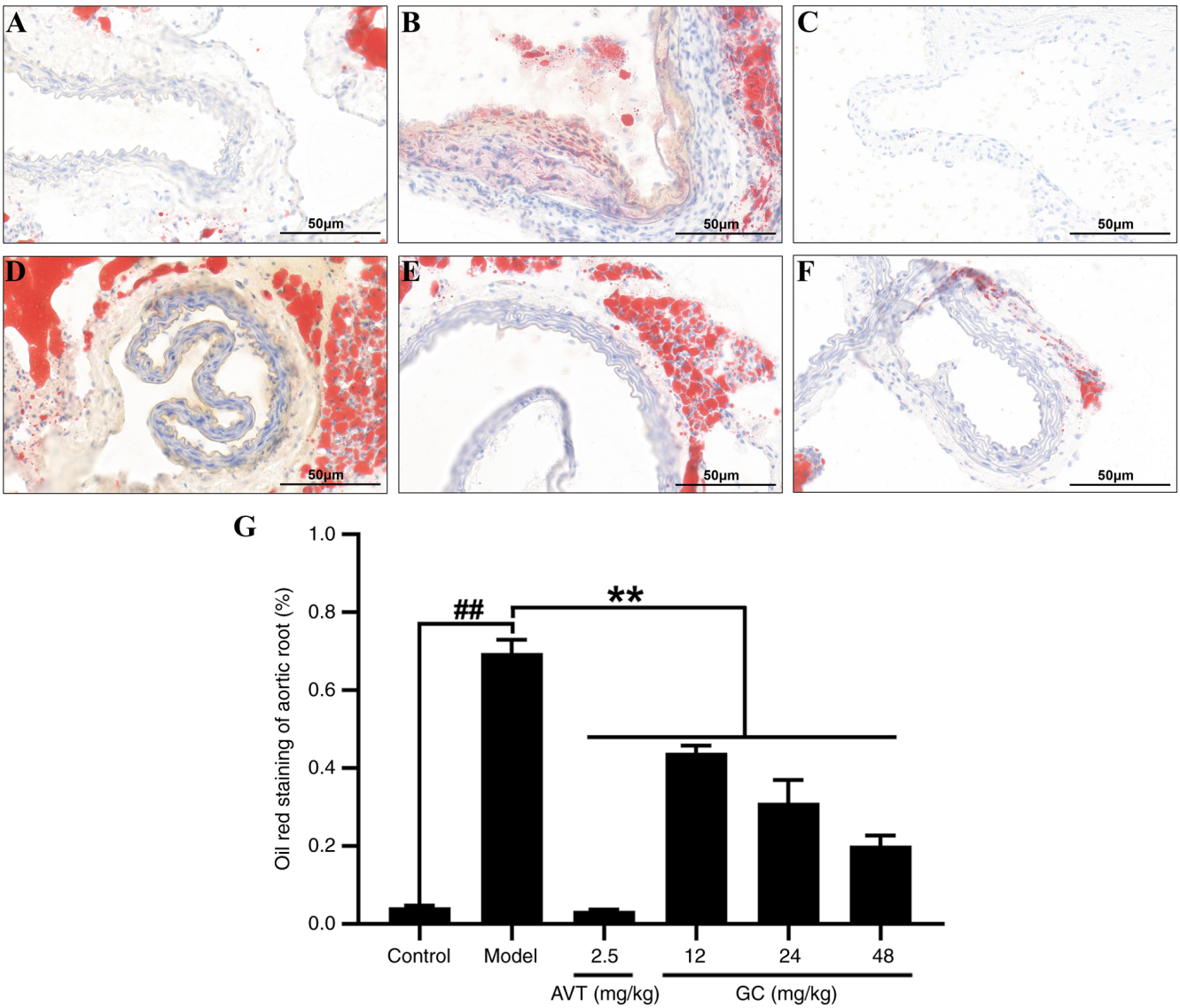

Figure 3. Effect of GC on lipid deposition of the aortic root via oil red O staining in atherosclerosis model mice. Light microscopy images (magnification, x40) of aortic roots stained with oil red O. (A) Control group, (B) model group, (C) 2.5 mg/kg AVT group, (D) 12 mg/kg GC group, (E) 24 mg/kg GC group and (F) 48 mg/kg GC group. (G) Quantitative analysis of atherosclerotic plaque area based on oil red O staining. Data are expressed as the mean ± SD. $^{\#\#}$P<0.01 vs. control group; **P<0.01 vs. model group. GC, ginkgolide C; AVT, atorvastatin.

extracellular matrix. Plaque cholesterol crystal dissolution with attenuated inflammatory infiltration indicates GC effectively reversed core pathological cascades of AS.

GC upregulates the expression levels of Nrf2 and its downstream antioxidant proteins HO-1, NQO1 and GCLM in AS model mice. As shown in Fig. 5A and B through IF analysis, Nrf2 expression demonstrated relatively low baseline levels in the control group. The model group exhibited marginal elevation in Nrf2 expression compared with the control group. However, GC administration at doses of 12, 24 and 48 mg/kg induced significant upregulation of Nrf2 expression levels (all P<0.01 vs. model group). Moreover, 2.5 mg/kg AVT slightly elevated the expression of Nrf2 (P<0.01 vs. model group). Furthermore, baseline expression levels of HO-1, NQO1 and GCLM were markedly diminished in the control group. While the model group demonstrated modest elevation of these antioxidant markers relative to controls, 12, 24, 48 mg/kg GC produced statistically significant inductions in HO-1, NQO1 and GCLM expression (Fig. 5C-E; all P<0.01 vs. model group).

GC downregulates the expression levels of NLRP3 and its downstream Caspase-1. As demonstrated in Fig. 6A-C, pathological activation of NLRP3 inflammasome components was significantly elevated in the model group, showing significant upregulation of both NLRP3 and Caspase-1. Conversely, GC treatment at ascending doses (12, 24, 48 mg/kg) exhibited progressive suppressions of NLRP3 and Caspase-1 (all P<0.01 vs. model group).

GC inhibits oxidative stress and inflammatory damage in AS model mice. Next, the effect of GC on the expression of inflammatory cytokines was further investigated in the serum of AS model mice. As revealed in Table II, the levels of IL-1β, IL-18 and TNF-α in the control group were low. After modeling, the levels of IL-1β, IL-18 and TNF-α increased to 361.85±62.80 pg/ml,

Table I. Effect of GC on serum lipid levels in atherosclerosis model mice.

Group	Dose (mg/kg)	TG (mM)	TC (mM)	LDL-C (mM)	HDL-C (mM)
Control		1.39±0.26	3.63±0.17	1.50±0.33	4.97±0.64
Model		5.58±0.26[b]	41.59±5.49[b]	16.14±2.41[b]	1.46±0.24[b]
AVT	2.5	1.53±0.36[a]	16.51±4.14[a]	1.67±0.62[a]	3.96±0.60[a]
GC	12	3.47±0.25[a]	26.45±2.18[a]	5.52±1.48[a]	2.72±0.84[a]
	24	2.71±0.39[a]	17.83±2.00[a]	4.30±1.51[a]	3.26±0.34[a]
	48	1.67±0.54[a]	11.75±1.23[a]	2.37±1.03[a]	4.44±0.54[a]

Values were expressed as the mean ± S.D. (n=6). [a]P<0.01 vs. model group; [b]P<0.01 vs. control group. GC, ginkgolide C; TG, triglycerides; TC, total cholesterol; LDL-C, low-density lipoprotein cholesterol; HDL-C, high-density lipoprotein cholesterol; AVT, atorvastatin.

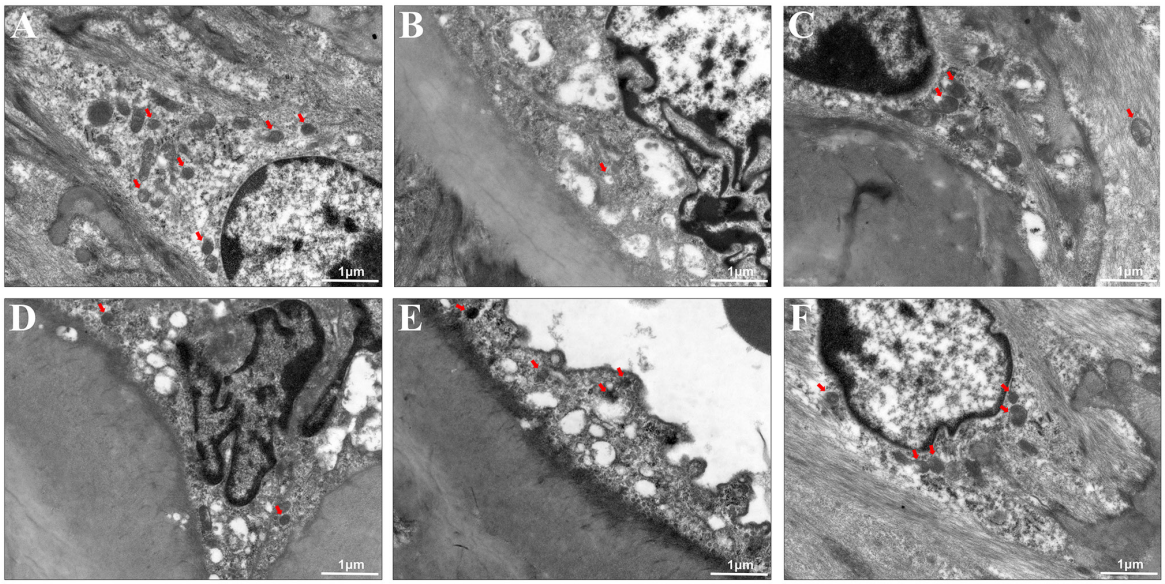

Figure 4. Transmission electron microscopy for ultrastructural changes in atherosclerosis model mice. (A) Control group, (B) model group, (C) 2.5 mg/kg AVT group, (D) 12 mg/kg GC group, (E) 24 mg/kg GC group and (F) 48 mg/kg GC group. AVT, atorvastatin; GC, ginkgolide C.

96.41±8.10 pg/ml, 97.90±6.64 pg/ml, respectively (all P<0.01 vs. control group). However, 2.5 mg/kg AVT and 12, 24, 48 mg/kg GC could dose-dependently reduced the expression levels of IL-1β, IL-18 and TNF-α (all P<0.01 vs. model group).

As demonstrated in Table III, the levels of SOD, MDA, LDH, CK, CAT, GSH and NADPH in the control group were 156.49±13.59 U/ml, 1.39±0.18 nM, 3513.01±663.44 U/l, 0.34±0.10 U/ml, 9.78±1.21 U/ml, 267.07±22.48 μM and 4.07±0.20 μM, respectively. After modeling, the cohort exhibited significant reductions in antioxidant defense markers (SOD, CAT and GSH) concomitant with significant elevations in oxidative stress indicators (MDA, LDH and CK) and NADPH generation (all P<0.01 vs. control group). 2.5 mg/kg AVT and 12, 24, 48 mg/kg GC significantly upregulated SOD, CAT and GSH while downregulating MDA, LDH, CK and NADPH, with all changes reaching statistical significance (P<0.05 vs. model group).

GC promotes cell survival, suppresses ROS generation, and inhibits apoptosis in ox-LDL-stimulated MAECs. As shown in Fig. 7A, ox-LDL-treated MAECs exhibited a significant reduction in cell viability (54.08±3.36%; P<0.01 vs. control group) as determined by MTT assay. Treatment of GC (1, 10, 100 μM) demonstrated dose-responsive enhancement of MAECs viabilities (68.11±8.67%, 76.05±4.71%, 86.19±5.11%, P<0.01 vs. model group).

Then, DCFDA was used for determining the level of ROS in MAECs (Fig. 7B). In contrast to the marked increase observed in ox-LDL-treated groups, ROS levels in the control group were substantially lower. In contrast to the model group, GC treatment at 1, 10 and 100 μM significantly reduced ROS levels (all P<0.01).

TUNEL staining result in Fig. 7C indicated that minimal apoptosis in control group, whereas the model group exhibited significant apoptotic cells. Treatment with 1, 10 and 100 μM GC markedly reduced apoptosis.

GC enhances Nrf2 nuclear translocation with upregulation of HO-1/NQO1/GCLM, while suppressing NLRP3/Caspase-1 expression. As revealed in Fig. 8A and B, Nrf2 was primarily localized in the cytoplasm with barely detectable nuclear levels in control cells. By contrast, ox-LDL stimulation promoted its

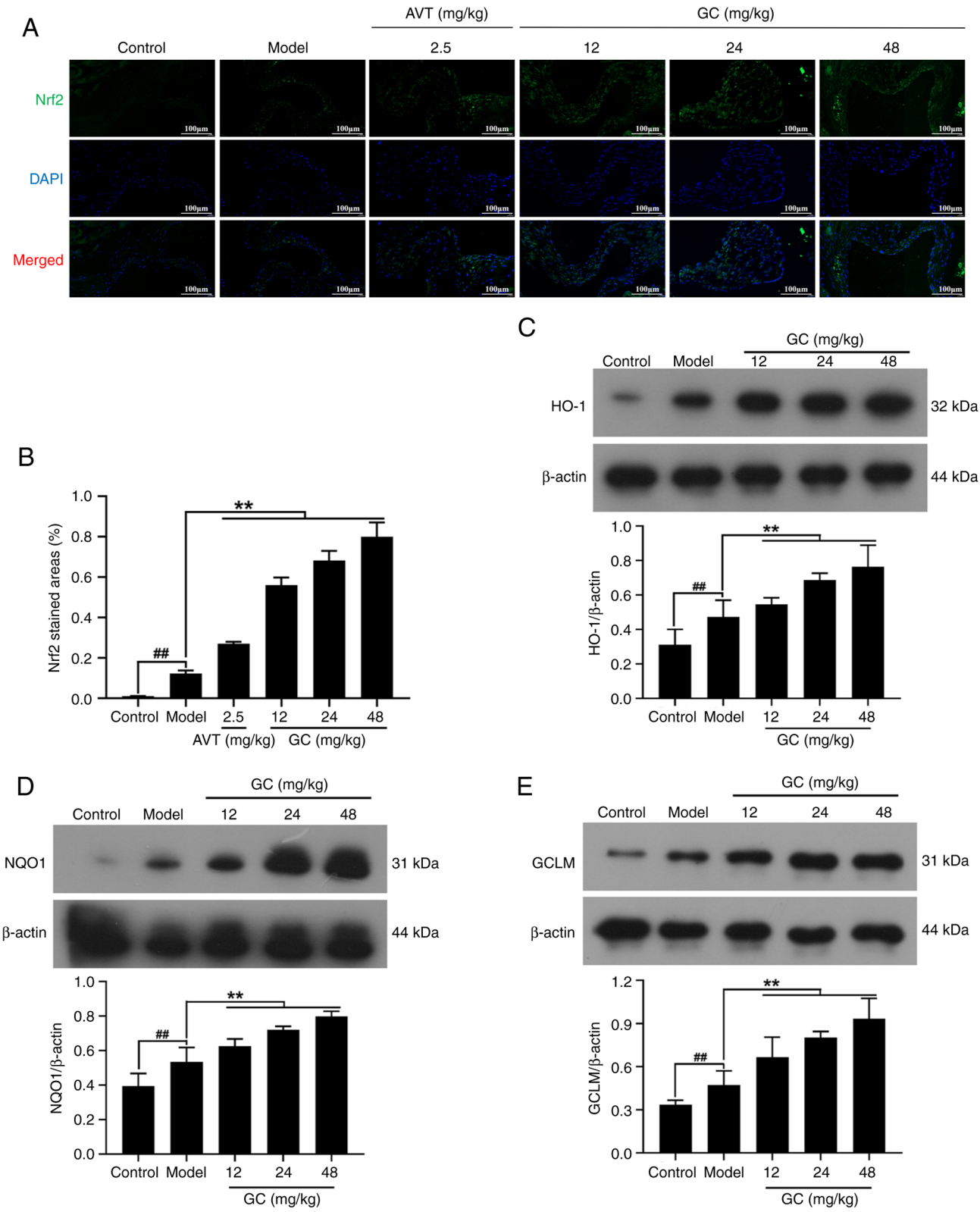

Figure 5. Effect of GC on Nrf2, HO-1, NQO1 and GCLM expression levels in atherosclerosis model mice. (A) Immunofluorescence staining was performed for measurement of Nrf2. (B) Quantitative analysis of Nrf2. (C-E) Western blot was applied to quantify the expression levels of (C) HO-1, (D) NQO1 and (E) GCLM. Results are expressed as protein/reference protein ratio. Data were expressed as the mean ± SD. $^{\#\#}$P<0.01 vs. control group; **P<0.01 vs. model group. GC, ginkgolide C; Nrf2, nuclear factor erythroid 2-related factor 2; HO-1, heme oxygenase-1; NQO1, NAD(P)H quinone oxidoreductase 1; GCLM, glutamate-cysteine ligase modifier subunit.

nuclear translocation. However, GC (1, 10, 100 μM) significantly enhanced the cytoplasmic-to-nuclear translocation of Nrf2. Therefore, GC significantly activated the Nrf2 signaling pathway, with increased cytoplasmic-to-nuclear translocation of Nrf2 leading to upregulation of HO-1, NQO1 and GCLM expression levels (Fig. 8C-E). The results in Fig. 8F and G

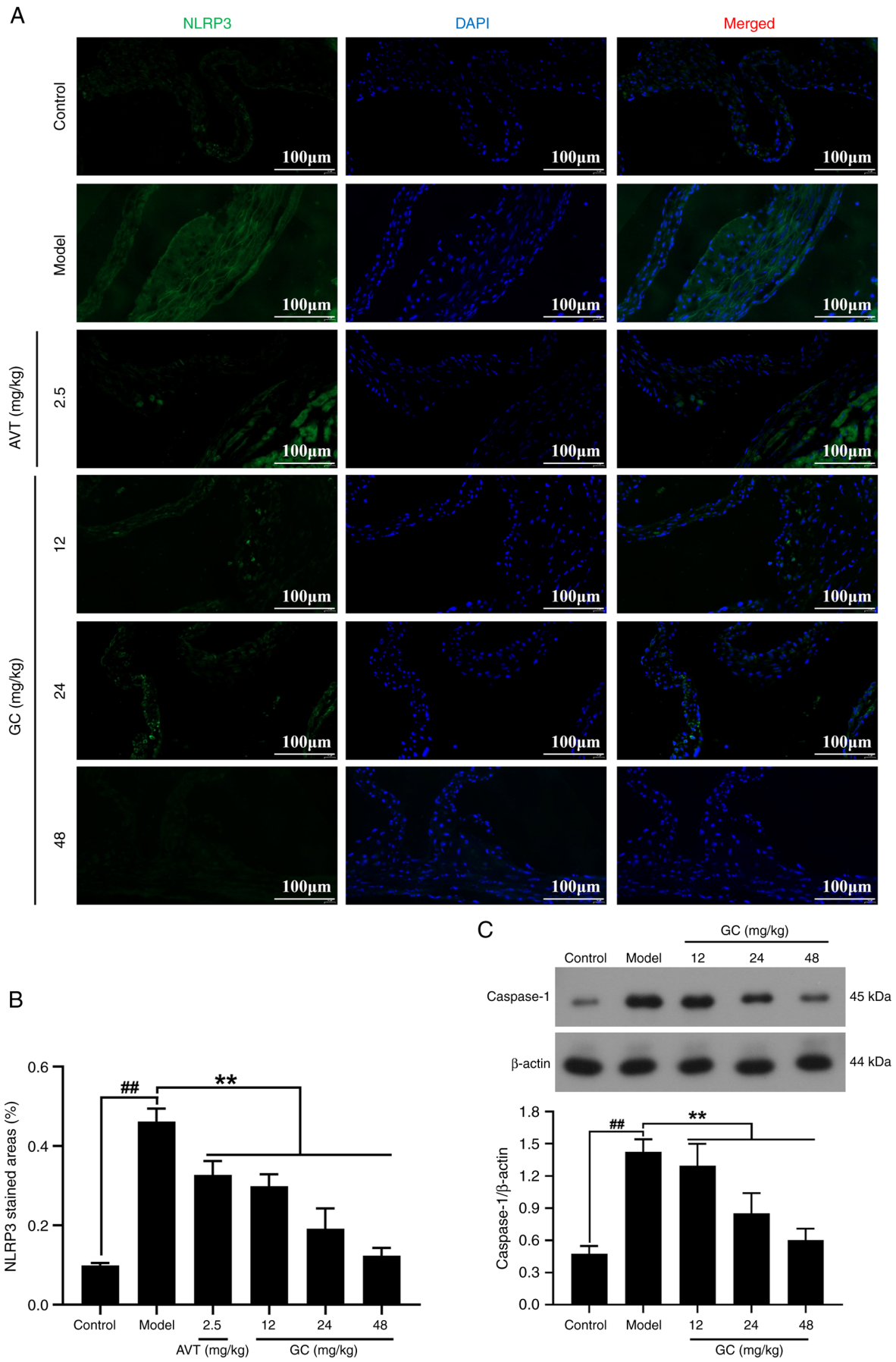

Figure 6. Effect of GC on NLRP3 and Caspase-1 expression levels in atherosclerosis model mice. (A) Immunofluorescence staining was performed for measurement of NLRP3. (B) Quantitative analysis of NLRP3. (C) Western blot was applied to quantify the expression of Caspase-1. Results were expressed as protein/reference protein ratio. Data are expressed as the mean ± SD. $^{\#\#}$P<0.01 vs. control group; **P<0.01 vs. model group. GC, ginkgolide C; NLRP3, Nod-like receptor protein 3.

Table II. Effect of GC on serum inflammatory cytokines in atherosclerosis model mice.

Group	Dose (mg/kg)	IL-1β (pg/ml)	IL-18 (pg/ml)	TNF-α (pg/ml)
Control		29.28±3.14	16.24±1.05	6.30±1.50
Model		361.85±62.80[b]	96.41±8.10[b]	97.90±6.64[b]
AVT	2.5	104.85±10.95[a]	59.46±6.90[a]	33.04±6.82[a]
GC	12	133.27±18.50[a]	57.47±2.07[a]	40.35±3.55[a]
	24	84.12±12.52[a]	28.25±8.88[a]	35.27±3.80[a]
	48	38.01±4.01[a]	17.52±2.27[a]	24.39±6.21[a]

Values are expressed as the mean ± S.D. (n=6). [a]P<0.01 vs. model group; [b]P<0.01 vs. control group. GC, ginkgolide C; AVT, atorvastatin; IL, interleukin; TNF, tumor necrosis factor.

Table III. Effect of GC on antioxidant enzymes in atherosclerosis model mice.

Group	Control	Model	AVT	GC		
Dose (mg/kg)			2.5	12	24	48
SOD (U/ml)	156.49±13.59	47.66±9.25[b]	82.01±4.51[a]	93.69±9.46[a]	101.95±6.02[a]	133.82±5.59[a]
MDA (nM)	1.39±0.18	8.10±0.60[b]	4.48±0.34[a]	4.20±0.67[a]	3.29±0.63[a]	2.37±0.26[a]
LDH (U/l)	3,513.01±663.44	9,953.69±510.21[b]	4,724.05±641.13[a]	6,460.10±728.44[a]	5,125.62±239.46[a]	4,242.19±692.69[a]
CK (U/ml)	0.34±0.10	1.37±0.22[b]	0.55±0.06[a]	0.89±0.14[a]	0.60±0.10[a]	0.48±0.05[a]
CAT (U/ml)	9.78±1.21	2.64±1.16[b]	6.10±0.73[b]	5.54±0.78[a]	6.50±1.23[a]	7.77±1.28[a]
GSH (μM)	267.07±22.48	79.55±15.10[b]	129.25±6.20[b]	133.67±21.23[a]	181.02±19.21[a]	219.30±15.46[a]
NADPH (μM)	4.07±0.20	8.20±0.25[b]	5.48±0.39[b]	5.90±0.39[a]	4.45±0.40[a]	4.10±0.73[a]

Values are expressed as the mean ± S.D. (n=6). [a]P<0.01 vs. model group; [b]P<0.01 vs. control group. GC, ginkgolide C; AVT, atorvastatin; SOD, superoxide dismutase; MDA, malondialdehyde; LDH, lactate dehydrogenase; CK, creatine kinase; CAT, catalase; GSH, glutathione.

showed that ox-LDL stimulation notably upregulated the expression of NLRP3 and Caspase-1. Whereas treatment of 1, 10 and 100 μM GC demonstrated dose-dependent suppression of NLRP3/Caspase-1 cascade activation.

GC also improves antioxidant capacity and suppresses inflammatory reaction in ox-LDL-stimulated MAECs. Results were consistent with *in vivo* experiments (Tables IV and V). ox-LDL exposure triggered concurrent elevation of pro-inflammatory cytokines (IL-1β, IL-18 and TNF-α) and oxidative markers (MDA, LDH, CK and NADPH), paralleled by significant depletion of antioxidant defenses (SOD, CAT and GSH) (all P<0.01 vs. control). However, 1, 10, and 100 μM GC could significantly improve the inflammatory response and oxidative stress damage induced by ox-LDL.

The data demonstrate a significant dual benefit of GC: It conferred a dose-dependent enhancement in oxidative stress tolerance concurrent with a suppression of inflammation. This effect, achievable through the potential activation of endogenous pathways such as Nrf2, highlights GC's role in simultaneously addressing two key pathological processes.

Discussion

CVDs remain the globally predominant cause of mortality, with AS serving as a central pathological driver (21). AS manifests as a multifactorial vascular pathology originating from disrupted endothelial homeostasis, clinically characterized by impaired vasomotor regulation, dyslipidemia, oxidative stress and chronic inflammatory cytokine activation (22,23). Exacerbated oxidative stress induces pathological ROS overproduction, elevating oxidative derivatives and provoking systemic oxidative damage. Subsequent pathological ROS accumulation directly activates the NLRP3 inflammasome, thereby potentiating proinflammatory cascades that exacerbate atherosclerotic lesion progression (24). Crucially, Nrf2, serving as a master regulator of redox homeostasis, negatively modulates NLRP3 inflammasome-mediated inflammation through redox-sensitive suppression of ROS-mediated signaling pathways (25). This mechanistic framework supports the author's hypothesis that GC attenuates atherosclerotic injury via Nrf2 activation-mediated ROS inhibition, consequently attenuating NLRP3 inflammasome activation and reducing atherosclerotic plaque progression.

Ginkgo biloba, a monotypic genus in the family Ginkgoaceae and the sole extant species of this lineage, is recognized as a 'living fossil' that occupies a pivotal node in plant evolutionary history (26,27). Modern pharmacological research demonstrates that the biological activity of *Ginkgo biloba* leaf extracts predominantly originates from its characteristic secondary metabolites, specifically terpene lactones (6%) and flavonoid glycosides (24%) as principal

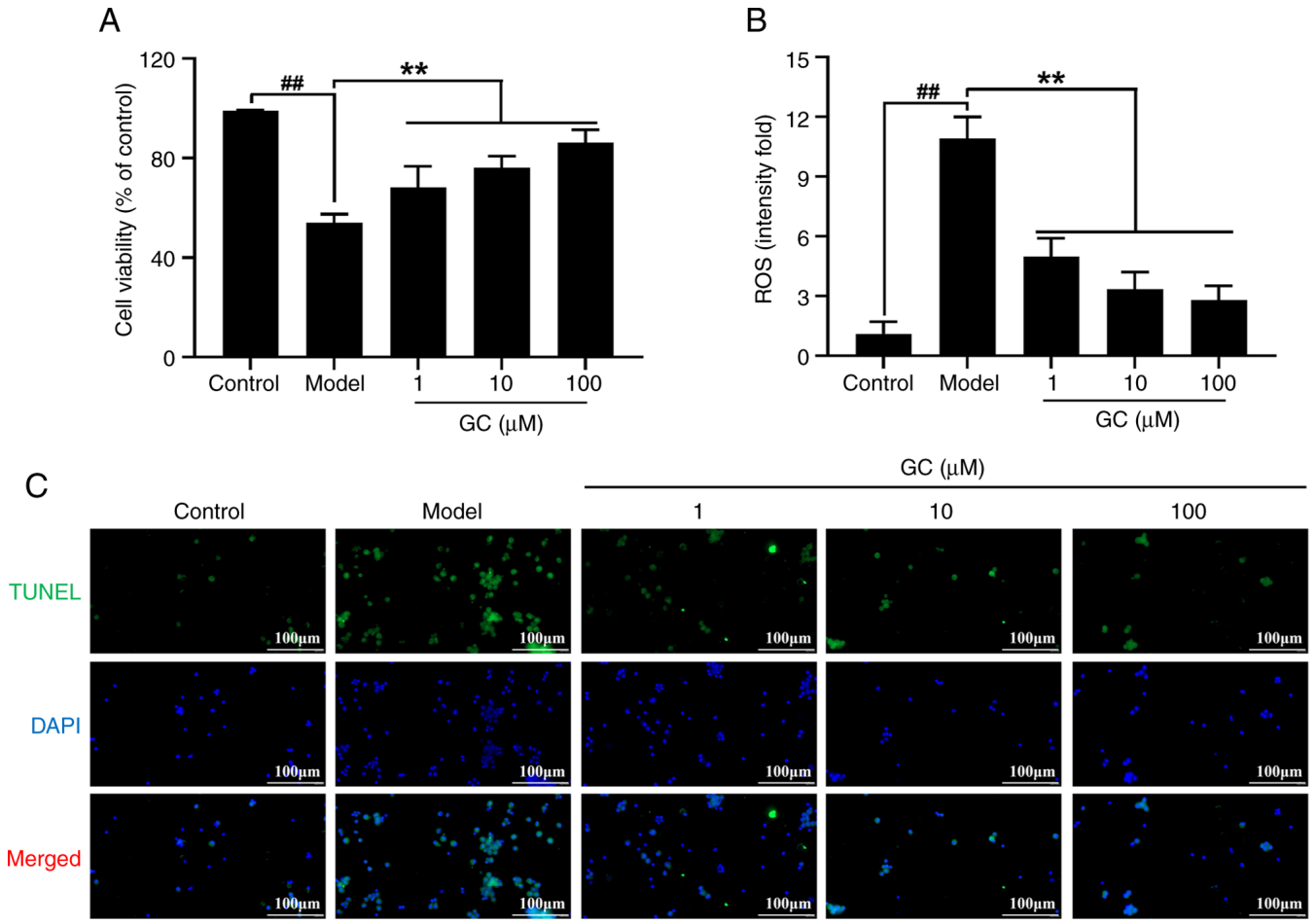

Figure 7. Effect of GC on cell viability, ROS production and cell apoptosis in oxidized-low density lipoprotein stimulated mouse aortic endothelial cells. (A) MTT assay was performed for measurement of cell viability. (B) ROS determination regent was used to quantify the level of ROS. (C) TUNEL staining was applied to evaluate the situation of cell apoptosis. Data are expressed as the mean ± SD. $^{\#\#}$P<0.01 vs. control group; **P<0.01 vs. model group. GC, ginkgolide C; ROS, reactive oxygen species.

active components. The latter category encompasses specific compounds such as ginkgolides A/B/C/J and bilobalide, whose unique diterpene trilactone molecular structure confers multi-target pharmacological activities (28). Guided by cumulative preclinical evidence, GC was designated as the lead therapeutic candidate. Experimental investigations employing *in vitro* and *in vivo* models have established that both isolated constituents manifest concentration-dependent cytoprotective efficacy against ischemia-reperfusion pathophysiology in both myocardial and cerebral compartments (18,19). The pathophysiological continuum of AS, constituting the common etiological substrate for cardio-cerebrovascular disorders, is mechanistically underpinned by dysregulated endothelial homeostasis, pathogenic leukocyte recruitment, and atheroma destabilization, pathobiological processes intrinsically linked to redox imbalance and dysregulated proinflammatory signaling pathways (29,30). Leveraging GC's multifaceted anti-inflammatory pharmacodynamics and multiphasic vascular protective actions, the present investigation systematically interrogates the compound's interactome within AS pathobiology, with dual objectives: i) Characterization of bioactive effector moieties governing its therapeutic efficacy, and ii) comprehensive mapping of pleiotropic therapeutic modalities encompassing atheroma stabilization, endothelial homeostatic restoration, and immunomodulatory microenvironment remodeling.

Of particular note is the atherogenic diet-fed ApoE$^{-/-}$ mouse model employed in the present study, which allowed for the evaluation of GC interventions under controlled, dose-escalating conditions. The experimental approach integrated serum lipid profiling, histological examination of plaques, and ultrastructural visualization via electron microscopy. Pathophysiologically, atherogenesis is widely understood to be initiated by dyslipidemia, wherein LDL-C undergoes oxidative modification to ox-LDL, triggering endothelial activation, inflammatory recruitment, and foam cell formation-central events in plaque development (31,32). Epidemiological observations consistently link hypercholesterolemia with increased cardiovascular risk, whereas HDL-C is recognized for its protective role via reverse cholesterol transport (33). In light of these established mechanisms, the lipid-modulating effects observed following GC intervention provide a substantive basis for discussing its potential therapeutic mechanism. The results suggest that GC may exert a dual regulatory influence, not only reducing atherogenic lipids but also promoting functional HDL activity, thereby contributing to the restoration of lipid homeostasis. This positions GC as a candidate for further investigation into its role in modulating key pathways involved

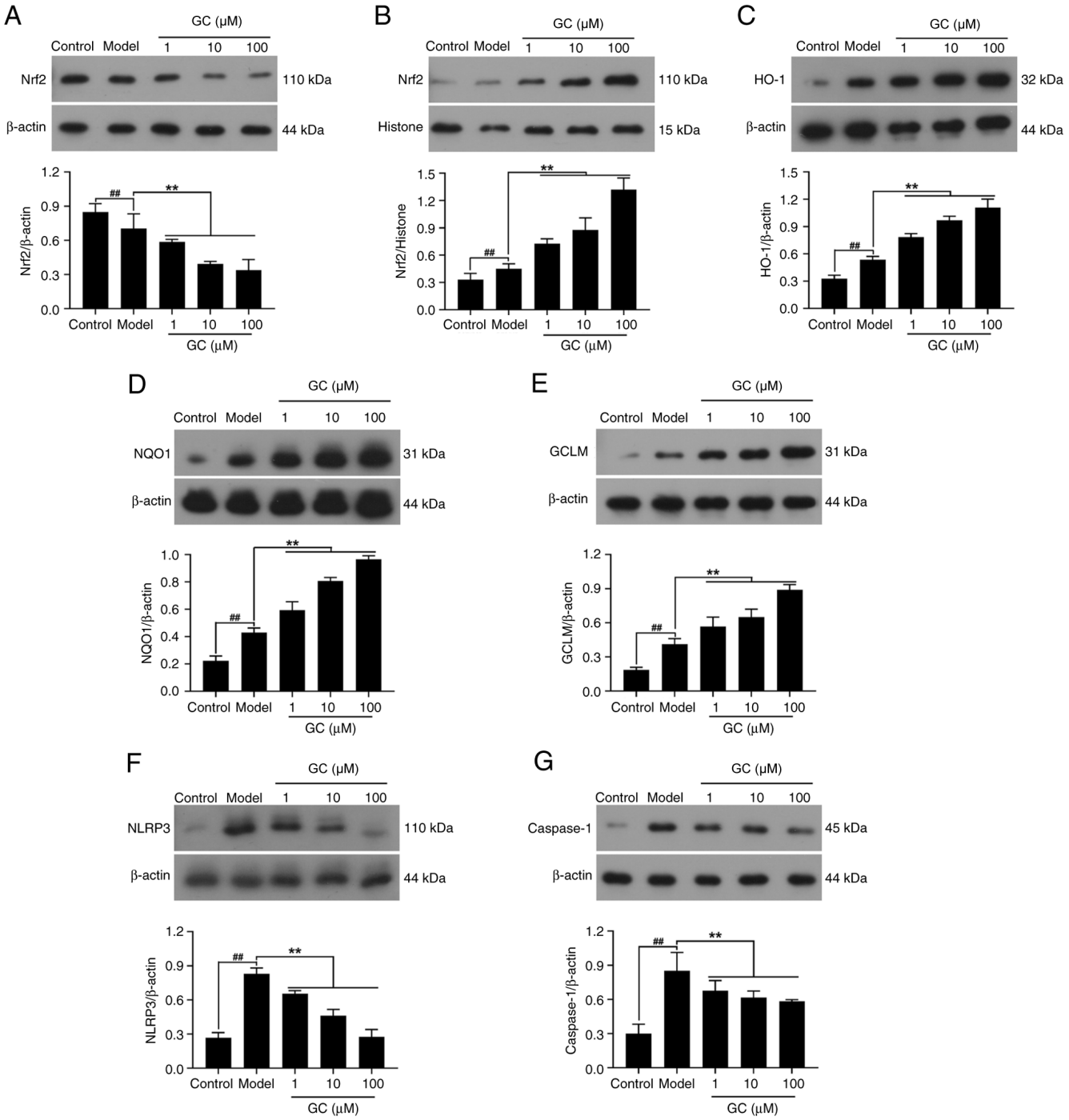

Figure 8. Effect of GC on expression levels of Nrf2, HO-1, NQO1, GCLM, NLRP3 and Caspase-1 in oxidized-low density lipoprotein stimulated mouse aortic endothelial cells. (A-G) Western blot was applied to quantify the expression levels of (A) cytoplasmic Nrf2, (B) nuclear Nrf2, (C) HO-1, (D) NQO1, (E) GCLM, (F) NLRP3 and (G) Caspase-1. Results were expressed as protein/reference protein ratio. Data are expressed as the mean ± SD. $^{\#\#}$P<0.01 vs. control group; **P<0.01 vs. model group. GC, ginkgolide C; Nrf2, nuclear factor erythroid 2-related factor 2; HO-1, heme oxygenase-1; NQO1, NAD(P)H quinone oxidoreductase 1; GCLM, glutamate-cysteine ligase modifier subunit; NLRP3, Nod-like receptor protein 3.

in AS progression. Notably, the pleiotropic modulation of both pro-atherogenic lipoprotein suppression and reverse cholesterol transport enhancement suggests GC's unique position in contemporary anti-atherosclerotic therapeutic strategies, potentially bridging current gaps in targeting complex lipid flux dysregulation. In the present study, GC was administered for only 7 days in a murine model of atherosclerotic lesions, yet AS is a chronic, long-term disease process. Whether GC can be sustainably used or possesses the potential to reverse atherosclerotic lesions remains unclear. Consequently, future studies are needed to systematically evaluate extended GC treatment regimens (for example, 6-12 weeks) to characterize its pharmacodynamic effects on plaque stabilization and regression.

The multifaceted antiatherogenic profile of GC warrants particular attention in the context of current therapeutic challenges. Rather than focusing solely on lipid reduction, GC appears to concurrently address plaque stabilization through

Table IV. Effect of GC on the supernatant inflammatory cytokines of oxidized-low density lipoprotein stimulated mouse aortic endothelial cells.

Group	Dose (μM)	IL-1β (pg/ml)	IL-18 (pg/ml)	TNF-α (pg/ml)
Control		1.80±0.53	11.73±2.90	6.94±1.47
Model		1,085.96±135.24[b]	121.00±19.23[b]	588.98±111.82[b]
GC	1	509.94±113.03[a]	34.43±5.09[a]	245.31±20.99[a]
	10	252.86±39.04[a]	21.12±6.34[a]	169.81±33.94[a]
	100	105.53±13.05[a]	12.27±1.34[a]	65.90±9.20[a]

Values are expressed as the mean ± S.D. (n=3). [a]P<0.01 vs. model group; [b]P<0.01 vs. control group. GC, ginkgolide C; IL, interleukin; TNF, tumor necrosis factor.

Table V. Effect of GC on antioxidant enzymes of oxidized-low density lipoprotein stimulated mouse aortic endothelial cells.

Group	Control	Model	GC		
Dose (μM)			1	10	100
SOD (U/mg pro)	296.04±24.49	129.08±23.70[b]	206.48±7.53[a]	241.78±8.70[a]	273.96±18.58[a]
MDA (nM/mg pro)	6.18±0.24	21.87±0.71[b]	15.91±1.66[a]	11.53±3.93[a]	9.39±1.77[a]
LDH (U/l)	702.27±38.14	1,257.27±212.96[b]	1,022.00±83.18[a]	891.48±38.90[a]	805.04±66.59[a]
CK (U/mg pro)	0.40±0.35	1.45±0.28[b]	1.01±0.41[a]	0.95±0.38[a]	0.83±0.21[a]
CAT (U/ml)	7.80±2.06	0.97±0.05[b]	2.38±0.58[a]	4.08±0.71[a]	6.17±0.38[a]
GSH (mg/g pro)	3.76±1.05	1.57±0.42[b]	2.45±0.41[a]	2.74±0.30[a]	3.22±0.19[a]
NADPH (μM)	9.72±2.52	34.60±4.18[b]	23.62±3.17[a]	16.51±0.54[a]	12.19±3.33[a]

Values are expressed as the mean ± S.D. (n=3). [a]P<0.01 vs. model group; [b]P<0.01 vs. control group. GC, ginkgolide C; SOD, superoxide dismutase; MDA, malondialdehyde; LDH, lactate dehydrogenase; CK, creatine kinase; CAT, catalase; GSH, glutathione.

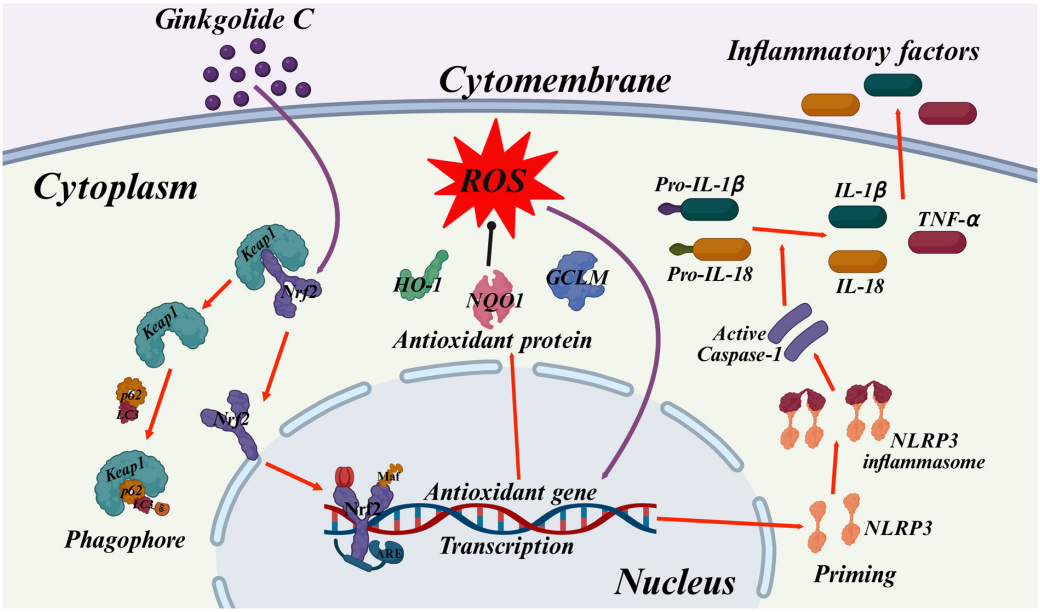

Figure 9. Elucidation of ginkgolide C-mediated inhibitory mechanisms in atherosclerosis pathogenesis. ROS, reactive oxygen species; NLRP3, Nod-like receptor protein 3; IL, interleukin; TNF, tumor necrosis factor.

collagenous cap preservation and endothelial restoration, as reflected in histopathological and ultrastructural observations. This suggests a synergistic mechanism that targets multiple pathological pathways-lipid retention, inflammatory signaling, and extracellular matrix degradation-which collectively contribute to atherosclerotic progression (34). Such a

multiphasic therapeutic approach may offer distinct advantages over conventional monotherapeutic strategies, particularly in its ability to intervene at both early and advanced stages of the disease (35). By reinforcing plaque microstructure and reducing lipid core vulnerability, GC holds potential clinical utility in managing high-risk plaques, especially in cases where statin therapy alone fails to mitigate persistent inflammatory risks. The convergence of these mechanisms supports GC's promise as a multimodal agent, meriting further investigation into its translational application in complex atherosclerotic disease.

The antioxidant properties of GC and their implications for AS management merit further discussion within the broader context of redox imbalance in CVD. Oxidative stress, characterized by disrupted redox homeostasis, plays a well-established role in driving endothelial dysfunction and plaque instability, largely through the persistent generation of ROS and subsequent lipid peroxidation (36). In this regard, GC appears to modulate key components of the oxidative cascade, influencing both the initiation and propagation of oxidative damage. Its potential to enhance endogenous antioxidant defenses while simultaneously mitigating peroxidative processes suggests a biphasic mechanism that may effectively disrupt the ROS-lipid oxidation-inflammatory axis, a critical pathway in AS progression. Notably, such a multitarget antioxidant strategy differs from conventional approaches by addressing oxidative stress at multiple levels, not only scavenging free radicals but also promoting enzymatic homeostasis (37). This may offer a more sustainable and physiologically integrated means of reducing oxidative injury in vascular tissues. Furthermore, the potential involvement of the Nrf2 pathway, as inferred from indirect evidence, hints at epigenetically mediated enhancement of cellular antioxidant capacity, positioning GC as a modulator of redox signaling beyond mere scavenging activity. Such pleiotropic regulation could be particularly relevant in clinical settings involving high residual oxidative stress, such as statin-resistant or advanced atherosclerotic cases, where monotherapeutic antioxidant strategies have shown limited success (38). These mechanistic insights encourage further investigation into GC's translational potential for preventing oxidative stress-driven cardiovascular events.

The central role of the Nrf2-ARE pathway in maintaining cellular redox homeostasis provides a compelling framework for discussing antioxidant-based interventions in AS. As a key transcriptional regulator, Nrf2 responds to oxidative stress by translocating to the nucleus and binding to ARE, thereby orchestrating the expression of cytoprotective genes (39,40). This mechanism enables a coordinated upregulation of endogenous defenses, which has attracted interest as a therapeutic strategy in vascular diseases driven by oxidative injury (41). Within this context, GC appears to engage the Nrf2-ARE axis, suggesting a capacity to modulate oxidative signaling beyond simple antioxidant scavenging. By potentially enhancing multiple defense mechanisms, such as HO-1-mediated detoxification, NQO1-regulated redox cycling and glutathione biosynthesis, GC may reinforce antioxidant capacity across cellular compartments, offering a more integrated approach to managing redox imbalance in AS.

Such multi-level regulation could be particularly advantageous in resolving the spatial and compositional heterogeneity of oxidative stress within atherosclerotic plaques (42,43). Unlike conventional monofunctional antioxidants, the potential epigenetic influence of GC on Nrf2 signaling may enable sustained modulation of redox homeostasis, positioning it as a candidate for addressing complex clinical scenarios, including statin-resistant cases where persistent oxidative stress contributes to residual cardiovascular risk. These considerations underscore the relevance of further exploring GC's role in targeting the interplay between oxidative stress, lipid metabolism and inflammation, key drivers of plaque progression and vulnerability.

The therapeutic strategy of concurrently targeting the NLRP3 inflammasome and potentiating the Nrf2 pathway represents a promising direction in AS research, particularly for disrupting the self-perpetuating cycle of oxidative stress, inflammation and lipid dysregulation (29,44). GC's putative dual modulation of these pathways suggests a capacity to intervene at multiple nodal points within the atherogenic cascade, not only by potentially mitigating oxidative triggers via Nrf2-mediated mechanisms but also by suppressing downstream inflammasome activation and cytokine release. Such an integrated approach may effectively uncouple the ROS-inflammation-lipid deposition triad, which is central to plaque progression and destabilization.

By simultaneously addressing oxidative insult and inflammatory amplification, GC could offer a therapeutic advantage over agents that target only single components of this pathogenic network. This may be especially relevant in advanced atherosclerotic lesions, where metabolic dysfunction and chronic inflammation coexist. The ability to stabilize plaque phenotype by modulating endothelial activation and attenuating leukocyte recruitment further highlights its potential vascular-protective role (45). From a clinical perspective, this bifunctional anti-inflammatory and antioxidant profile may hold particular value in managing complex patient subsets, such as those with pyroptosis-prone plaques or inadequate responses to conventional lipid-lowering therapy, underscoring the need for further investigation into its translational applicability (46,47).

Collectively, this investigation mechanistically demonstrates GC-mediated cytoprotection against AS through Nrf2-dependent redox homeostasis modulation, concomitantly attenuating NLRP3 inflammasome activation and downstream pro-inflammatory effector signaling (Fig. 9). These findings establish a preclinical rationale for advancing *Ginkgo biloba* bioactive constituents as multi-mechanistic therapeutics in atherosclerotic CVD management.

Acknowledgements

Not applicable.

Funding

No funding was received.

Availability of data and materials

The data generated in the present study may be requested from the corresponding author.

Authors' contributions

RZ conducted investigation, formal analysis, conceptualization, developed methodology, acquired funding, curated and visualized data, wrote, reviewed and edited the manuscript. The author read and approved the final version of the manuscript. RZ confirms the authenticity of all the raw data.

Ethics approval and consent to participate

The present study was approved by the Ethics Committee of the Shandong Provincial Hospital Affiliated to Shandong First Medical University (approval no. 2022-661; Jinan, China).

Patient consent for publication

Not applicable.

Competing interests

All authors declare that they have no competing interests.

References

1. Boffa MB and Koschinsky ML: Lipoprotein(a) and cardiovascular disease. Biochem J 481: 1277-1296, 2024.
2. Lusis AJ: Atherosclerosis. Nature 407: 233-241, 2000.
3. Hassan HA, Ahmed HS and Hassan DF: Free radicals and oxidative stress: Mechanisms and therapeutic targets. Hum Antibodies 32: 151-167, 2024.
4. Aleksandrowicz M, Konop M, Rybka M, Mazurek Ł, Stradczuk-Mazurek M, Kciuk M, Bądzyńska B, Dobrowolski L and Kuczeriszka M: Dysfunction of microcirculation in atherosclerosis: Implications of nitric oxide, oxidative stress, and inflammation. Int J Mol Sci 26: 6467, 2025.
5. Batty M, Bennett MR and Yu E: The role of oxidative stress in atherosclerosis. Cells 11: 3843, 2022.
6. Jakubowski H and Witucki Ł: Homocysteine metabolites, endothelial dysfunction, and cardiovascular disease. Int J Mol Sci 26: 746, 2025.
7. Zhu L, Liao Y and Jiang B: Role of ROS and autophagy in the pathological process of atherosclerosis. J Physiol Biochem 80: 743-756, 2024.
8. Howden R: Nrf2 and cardiovascular defense. Oxid Med Cell Longev 2013: 104308, 2013.
9. Jomova K, Raptova R, Alomar SY, Alwasel SH, Nepovimova E, Kuca K and Valko M: Reactive oxygen species, toxicity, oxidative stress, and antioxidants: Chronic diseases and aging. Arch Toxicol 97: 2499-2574, 2023.
10. Mimura J and Itoh K: Role of Nrf2 in the pathogenesis of atherosclerosis. Free radical biology & medicine 88: 221-232, 2015.
11. O'Rourke SA, Shanley LC and Dunne A: The Nrf2-HO-1 system and inflammaging. Front Immunol 15: 1457010, 2024.
12. Grebe A, Hoss F and Latz E: NLRP3 Inflammasome and the IL-1 pathway in atherosclerosis. Circ Res 122: 1722-1740, 2018.
13. Wang K, Liu H, Sun W, Guo J, Jiang Z, Xu S and Miao Z: Eucalyptol alleviates avermectin exposure-induced apoptosis and necroptosis of grass carp hepatocytes by regulating ROS/NLRP3 axis. Aquat Toxicol 264: 106739, 2023.
14. Fu J and Wu H: Structural mechanisms of NLRP3 inflammasome assembly and activation. Annu Rev Immunol 41: 301-316, 2023.
15. Tall AR and Bornfeldt KE: Inflammasomes and atherosclerosis: A mixed picture. Circ Res 132: 1505-1520, 2023.
16. Hort J, Duning T and Hoerr R: *Ginkgo biloba* Extract EGb 761 in the treatment of patients with mild neurocognitive impairment: A systematic review. Neuropsychiatr Dis Treat 19: 647-660, 2023.
17. Boateng ID: Ginkgols and bilobols in *Ginkgo biloba* L. A review of their extraction and bioactivities. Phytother Res 37: 3211-3223, 2023.
18. Zhang R, Han D, Li Z, Shen C, Zhang Y, Li J, Yan G, Li S, Hu B, Li J and Liu P: Corrigendum: Ginkgolide C alleviates myocardial ischemia/reperfusion-induced inflammatory injury via inhibition of CD40-NF-κB pathway. Front Pharmacol 15: 1492520, 2024.
19. Li B, Zhang B, Li Z, Li S, Li J, Wang A, Hou J, Xu J and Zhang R: Ginkgolide C attenuates cerebral ischemia/reperfusion-induced inflammatory impairments by suppressing CD40/NF-κB pathway. J Ethnopharmacol 312: 116537, 2023.
20. Emanueli C, Schmidt AM and Golledge J: Unveiling intriguing links between limb ischemia, systemic inflammation, and progressive atherosclerosis: A tangled and interconnected web. Arterioscler Thromb Vasc Biol 43: 907-909, 2023.
21. Tasouli-Drakou V, Ogurek I, Shaikh T, Ringor M, DiCaro MV and Lei K: Atherosclerosis: A comprehensive review of molecular factors and mechanisms. Int J Mol Sci 26: 1364, 2025.
22. Wang X, Shen Y, Shang M, Liu X and Munn LL: Endothelial mechanobiology in atherosclerosis. Cardiovasc Res 119: 1656-1675, 2023.
23. Yang DR, Wang MY, Zhang CL and Wang Y: Endothelial dysfunction in vascular complications of diabetes: A comprehensive review of mechanisms and implications. Front Endocrinol (Lausanne) 15: 1359255, 2024.
24. He B, Nie Q, Wang F, Wang X, Zhou Y, Wang C, Guo J, Fan X, Ye Z, Liu P and Wen J: Hyperuricemia promotes the progression of atherosclerosis by activating endothelial cell pyroptosis via the ROS/NLRP3 pathway. J Cell Physiol 238: 1808-1822, 2023.
25. Zhang B, Yu J, Bao L, Feng D, Qin Y, Fan D, Hong X and Chen Y: Cynarin inhibits microglia-induced pyroptosis and neuroinflammation via Nrf2/ROS/NLRP3 axis after spinal cord injury. Inflamm Res 73: 1981-1994, 2024.
26. Lin J, Sun X and Yang L: Effects and safety of *Ginkgo biloba* on depression: A systematic review and meta-analysis. Front Pharmacol 15: 1364030, 2024.
27. Fang WH, Bonavida V, Agrawal DK and Thankam FG: Hyperlipidemia in tendon injury: Chronicles of low-density lipoproteins. Cell Tissue Res 392: 431-442, 2023.
28. Silva H and Martins FG: Cardiovascular activity of *Ginkgo biloba*-An insight from healthy subjects. Biology (Basel) 12: 15, 2022.
29. Kong P, Cui ZY, Huang XF, Zhang DD, Guo RJ and Han M: Inflammation and atherosclerosis: Signaling pathways and therapeutic intervention. Signal Transduct Target Ther 7: 131, 2022.
30. Weber C, Habenicht AJR and von Hundelshausen P: Novel mechanisms and therapeutic targets in atherosclerosis: Inflammation and beyond. Eur Heart J 44: 2672-2681, 2023.
31. Zhang S, Hong F, Ma C and Yang S: Hepatic lipid metabolism disorder and atherosclerosis. Endocr Metab Immune Disord Drug Targets 22: 590-600, 2022.
32. Lubrano V, Ndreu R and Balzan S: Classes of lipid mediators and their effects on vascular inflammation in atherosclerosis. Int J Mol Sci 24: 1637, 2023.
33. Bu LL, Yuan HH, Xie LL, Guo MH, Liao DF and Zheng XL: New dawn for atherosclerosis: Vascular endothelial cell senescence and death. Int J Mol Sci 24: 15160, 2023.
34. Pintó X, Fanlo M, Esteve V and Millán J: Remnant cholesterol, vascular risk, and prevention of atherosclerosis. Clin Investig Arterioscler 35: 206-217, 2023.
35. Gaggini M, Gorini F and Vassalle C: Lipids in atherosclerosis: Pathophysiology and the role of calculated lipid indices in assessing cardiovascular risk in patients with hyperlipidemia. Int J Mol Sci 24: 75, 2022.
36. Dabravolski SA, Churov AV, Beloyartsev DF, Kovyanova TI, Lyapina IN, Sukhorukov VN and Orekhov AN: The role of NRF2 function and regulation in atherosclerosis: An update. Mol Cell Biochem 480: 3935-3949, 2025.
37. Jomova K, Alomar SY, Valko R, Liska J, Nepovimova E, Kuca K and Valko M: Flavonoids and their role in oxidative stress, inflammation, and human diseases. Chem Biol Interact 413: 111489, 2025.
38. Yan Q, Liu S, Sun Y, Chen C, Yang S, Lin M, Long J, Yao J, Lin Y, Yi F, *et al*: Targeting oxidative stress as a preventive and therapeutic approach for cardiovascular disease. J Transl Med 21: 519, 2023.
39. Zhang Z, Dai Y, Xiao Y and Liu Q: Protective effects of catalpol on cardio-cerebrovascular diseases: A comprehensive review. J Pharm Anal 13: 1089-1101, 2023.
40. Han H, Zhang G, Zhang X and Zhao Q: Nrf2-mediated ferroptosis inhibition: A novel approach for managing inflammatory diseases. Inflammopharmacology 32: 2961-2986, 2024.

41. Meng T, Li X, Li C, Liu J, Chang H, Jiang N, Li J, Zhou Y and Liu Z: Natural products of traditional Chinese medicine treat atherosclerosis by regulating inflammatory and oxidative stress pathways. Front Pharmacol 13: 997598, 2022.
42. Huang Z, Wu M, Zeng L and Wang D: The beneficial role of Nrf2 in the endothelial dysfunction of atherosclerosis. Cardiol Res Pract 2022: 4287711, 2022.
43. Pfefferlé M and Vallelian F: Transcription factor NRF2 in shaping myeloid cell differentiation and function. Adv Exp Med Biol 1459: 159-195, 2024.
44. Zhang XN, Yu ZL, Chen JY, Li XY, Wang ZP, Wu M and Liu LT: The crosstalk between NLRP3 inflammasome and gut microbiome in atherosclerosis. Pharmacol Res 181: 106289, 2022.
45. Tanase DM, Valasciuc E, Gosav EM, Ouatu A, Buliga-Finis ON, Floria M, Maranduca MA and Serban IL: Portrayal of NLRP3 inflammasome in atherosclerosis: Current knowledge and therapeutic targets. Int J Mol Sci 24: 8162, 2023.
46. Zhang H and Dhalla NS: The role of Pro-inflammatory cytokines in the pathogenesis of cardiovascular disease. Int J Mol Sci 25: 1082, 2024.
47. Asemi R, Omidi Najafabadi E, Mahmoudian Z, Reiter RJ, Mansournia MA and Asemi Z: Melatonin as a treatment for atherosclerosis: Focus on programmed cell death, inflammation and oxidative stress. J Cardiothorac Surg 20: 194, 2025.